NEOPLASIA
www.neoplasia.com
Volume 31 Number xxx Month 2022 pp. 100816

Original Research

IGDQ motogenic peptide gradient induces directional cell migration through integrin $(\alpha v)\beta 3$ activation in MDA-MB-231 metastatic breast cancer cells ☆

Sophie Ayama-Canden [a]; Rodolfo Tondo [b]; Liliana Piñeros [a]; Noëlle Ninane [a]; Catherine Demazy [a]; Marc Dieu [d]; Antoine Fattaccioli [a]; Tijani Tabarrant [e]; Stéphane Lucas [e]; Davide Bonifazi [b,c]; Carine Michiels [a,*]

[a] URBC – NARILIS, University of Namur, rue de Bruxelles 61, 5000 Namur, Belgium
[b] School of Chemistry, Cardiff University, Park Place, Main Building, CF10 3AT, Cardiff, Wales, United Kingdom
[c] Institute of Organic Chemistry, University of Vienna, Währinger Str. 38, 1090 Vienna, Austria
[d] MaSUN, Mass Spectrometry Facility, University of Namur, 61, rue de Bruxelles, 5000 Namur, Belgium
[e] LARN – NARILIS, University of Namur, rue de Bruxelles 61, 5000 Namur, Belgium

Abstract

In the context of breast cancer metastasis study, we have shown in an *in vitro* model of cell migration that IGDQ-exposing (IsoLeu-Gly-Asp-Glutamine type I Fibronectin motif) monolayers (SAMs) on gold sustain the adhesion of breast cancer MDA-MB-231 cells by triggering Focal Adhesion Kinase and integrin activation. Such tunable scaffolds are used to mimic the tumor extracellular environment, inducing and controlling cell migration. The observed migratory behavior induced by the IGDQ-bearing peptide gradient along the surface allows to separate cell subpopulations with a "stationary" or "migratory" phenotype. In this work, we knocked down the integrins $\alpha 5(\beta 1)$ and $(\alpha v)\beta$ since they are already known to be implicated in cell migration. To this aim, a whole proteomic analysis was performed in beta 3 integrin (ITGB3) or alpha 5 integrin (ITGA5) knock-down MDA-MB-231 cells, in order to highlight the pathways implied in the integrin-dependent cell migration.
Our results showed that i) ITGB3 depletion influenced ITGA5 mRNA expression, ii) ITGB3 and ITGA5 were both necessary for IGDQ-mediated directional single cell migration and iii) integrin $(\alpha v)\beta 3$ was activated by IGDQ fibronectin type I motif. Finally, the proteomic analysis suggested that co-regulation of recycling transport of ITGB3 by ITGA5 is potentially necessary for directional IGDQ-mediated cell migration.

Neoplasia (2022) 31, 100816

Keywords: Breast cancer, TNBC, Cell migration, Motogenic IGDQ motif, Fibronectin type I, Integrin alpha 5, Integrin beta 3

Introduction

The poor prognosis of breast cancer is mainly due to metastasis formation. All stages combined, survival at 5 years is 90% for breast cancer. For triple negative breast cancer the survival rate at 5 years drop to 77% all stages combined and to 12% when a distant metastasis is detected [1]. Metastasis formation is a multistep process in which cancer cells migrate out of the primary tumors and form secondary tumors in distant sites. Cell migration is a complex mechanism crucial for many physiological and pathological processes including tissue regeneration, immune response and cancer progression [2–5].

Multiple elements modulate cancer cell migration including the tumor microenvironment composed of immune cells, endothelial cells, fibroblasts, soluble elements (chemotaxis) and interaction with the extracellular matrix (ECM - haptotaxis) [6]. Cancer cell migration occurs through different processes, divided in two subtypes: collective cell migration and single cell migration [7]. In collective migration, cells migrate in multicellular strands

* Corresponding author.
E-mail address: carine.michiels@unamur.be (C. Michiels).
☆ Declaration of Competing Interest: The authors declare no competing interests.
Received 3 October 2021; received in revised form 8 June 2022; accepted 13 June 2022

https://doi.org/10.1016/j.neo.2022.100816

or in sheets when transformed cells are invasive but not yet metastatic, as observed in some epithelial cancers. In later stages, cell clusters can detach, disseminate and initiate metastasis locally, as observed in melanomas, breast, colon and prostate cancers. Single cancer cell migration occurs as mesenchymal-cell like migration or with an amoeboid behavior. The type of cancer cell migration is influenced by the cancer type, cell-ECM and cell-cell interactions. In general, the structure, composition and physical properties of the ECM [8] highly influence cell migration through durotaxis, haptotaxis and contact guidance. Hence, the interplay and crosstalk in the composition of the ECM also play a major role in the regulation and the behavior of cells, especially during migration [9–11].

Cells can detect chemical and physical gradients [12,13], both on surfaces and in solution, and respond to them with oriented movement [14]. Indeed, cell motility is affected by chemoattractant such as Epithelial Growth Factor (EGF), Transforming Growth Factor (TGF-β), collagen and fibronectin (Fn). It was previously shown, in a microfluidic system, that the oriented cell migration of breast cancer cells depends not only on the gradient profile but also on the range of EGF concentrations [15]. Furthermore, Fn precisely modulates cell migration. This process occurs through its interaction with specific transmembrane proteins, the integrins. The insoluble cellular dimer fibronectin entangles with other ECM insoluble components such as collagen, fibrin and laminin fibers, hence forming a major constituant of the insoluble ECM [16]. It is mainly produced by fibroblasts (stromal cells), but it is also synthetized by cancer cells themselves. Multiple variants of fibronectin exist, expressed from a single pre-mRNA, spliced to generate 20 variants in human [17,18]. Hence, fibronectin isoforms carry different modules containing peptidic motifs, which can induce specific biological processes via the activation of specific integrins (Figure 1-A). The type and abundance of the three types of Fn in the ECM depend on local and global microenvironment context, promoting or not cell survival, proliferation and migration [17]. The fibronectin is subdivided into domains. Fn domains are subdivided into modules and modules contain specific peptidic motifs (Figure 1-A). The type I Fn module contains IGD units (Q or S), which are motogenic [19]. These motifs can activate integrins and induce cell migration. The type II Fn module mostly participates in cell adhesion to ECM [20]. It also contains domains for fibrin and collagen binding. Type II Fn module is the collagen-binding domain. The minimum domain size contains one module type I Fn and two modules type II Fn [21]. Type III Fn module is the most abundant one and is the most studied until now. It contains fibulin-1, heparin and syndecan binding domains [22]. It also contains the RGD motif which promotes cell proliferation and adhesion by triggering specific integrin activation and cell signaling cascade response, through focal adhesion formation [23,24].

Until now, the interplay between specific integrin-mediated ECM adhesion and directional single cell migration is not well understood. In particular, the efforts to understand and guide cellular migration have led to the development of various approaches to generate confined and surface-immobilized chemical gradients able to mimic natural 3D environment and control cell migration *in vitro* [25]. Several works reported the use of Fn fragments in combination with mixed self assembly monolayers (SAMs) of alkanethiols to promote the biospecific attachment of cells through the integrin-based recognition [26,27]. Upon demonstrating that low concentrations of GBD (gelatin binding domain) stimulate the migration of human dermal fibroblasts into 3D-gels of native type I collagen fibers [28], Schor et al attributed the biological activity of GBD to the highly conserved Isoleucine-Glycine-Aspartic acid (IGD) motif of Fn [19,29,30]. In order to characterize the oriented migratory phenotype, we previously developed SAMs exposing gradients of IGDQ gradients [31] (Figure 1 B–C). We could thus identify two cell subpopulations associated either with a "stationary" phenotype or with a "migratory" phenotype, the latter determining a considerable cell migration at the sub-cm length scale [31] (Figure 1-C). One of the main limitation to analyze the gene expression of metastatic cells and to identify the pathways involved in metastasis formation was the segregation of the non-migrating cells from those displaying migrating aptitude without losing their phenotype. Our engineered surfaces presented a response to that limitation.

Building on these discoveries, we focused on the understanding of the role of integrins $\alpha5\beta1$ and $\alpha v\beta3$ in the recognition with IGDQ, since they are described as essential for cell migration and invasion [2,32]. Integrins are transmembrane proteins formed by two subunits, one alpha and one beta (Figure 2-A). Each integrin or group of integrins can interact with different elements of the ECM, including fibronectin, collagens or laminins (Figure 2-A). In order to evaluate and characterize the biological migration process induced by the motogenic motif IGDQ through integrin activation, the breast cancer cell line MDA-MB-231 was used. This cell line is epithelial with a mesenchymal-like phenotype that has already undergone the EMT and is frequently used to study cell migration and metastasis formation. Moreover, this cell line constitutively expresses both $\alpha5(\beta1)$ and $(\alpha v)\beta3$ integrins.

With the aim to unravel pathways involved in integrin-dependent cancer cell migration and the motogenic activity of the IGDQ sequence in metastatic processes, we a) studied the role and interaction of $\alpha5(\beta1)$ and $(\alpha v)\beta3$ integrins in a wound healing assay and in single cell migration and b) performed a proteomic analysis coupled to bioinformatics analyses. Altogether, the results identified new integrin-dependent pathways that regulate the migration process using a complete proteomic analysis.

Results

Beta 3 integrin depletion influences integrin alpha 5 expression

To investigate the role of $\alpha5\beta1$ and $\alpha v\beta3$ in cell migration, a constitutive knock-down strategy for alpha 5 (ITGA5) and beta 3 (ITGB3) integrin subunits, using shRNA-expressing vectors, was used in MDA-MB-231 metastatic breast cancer cells. Indeed, ITGA5 only can dimerize with ITGB1 and ITGB3 with ITGAV. RNA knock-down efficiency was evaluated by measuring mRNA level using qPCR (Figure 2–B) and protein level using western blotting (Figure 2–D–E) and immunofluorescence labeling (Supplemental Figure 1–C–D). ITGA5 and ITGB3 knock-down did not show any significant impact on ITGAv and ITGB1 mRNA expression (Figure 2–C), nor protein abundance as assessed from the mass spectrometry proteomic data (data not shown). shITGA5-126 led to an efficient knock-down with a decrease in ITGA5 mRNA level of 62 % ($p < 0.1$) and in protein of abundance 72.7 % ($p < 0.001$). This knock-down was used because we observed that higher knock-down level induced cell detachment due to the well-known involvement of ITGA5 in cell adhesion, thus making impossible the use of such cells for experiments.

For shITGB3-237, a decrease of ITGB3 83 % in mRNA level ($p < 0.01$) and of 81.1 % in protein abundance ($p < 0.001$) were obtained. These results were confirmed by immunofluorescence labeling (Supplemental Figure 1–C–D). These results were confirmed using another shRNA for ITGB3 (Supplemental Figure 2).

Interestingly, ITGA5 expression increased in ITGB3-knock-down cells at both RNA and protein levels (Figure 2–B–C–D–Supplemental Figure 1 C). This suggests an indirect negative transcriptional regulation of ITGA5 by ITGB3 expression, while the reverse was not observed.

Regarding proliferation, no significant difference was observed in knock-down cells compared to control cells (shCTL – Supplemental Figure 1–A–B) and no cytotoxic effect of shRNAs was demonstrated (LDH assays – data not shown). This suggests that ITGA5 or ITGB3 depletion has no deleterious impact on cell cycle.

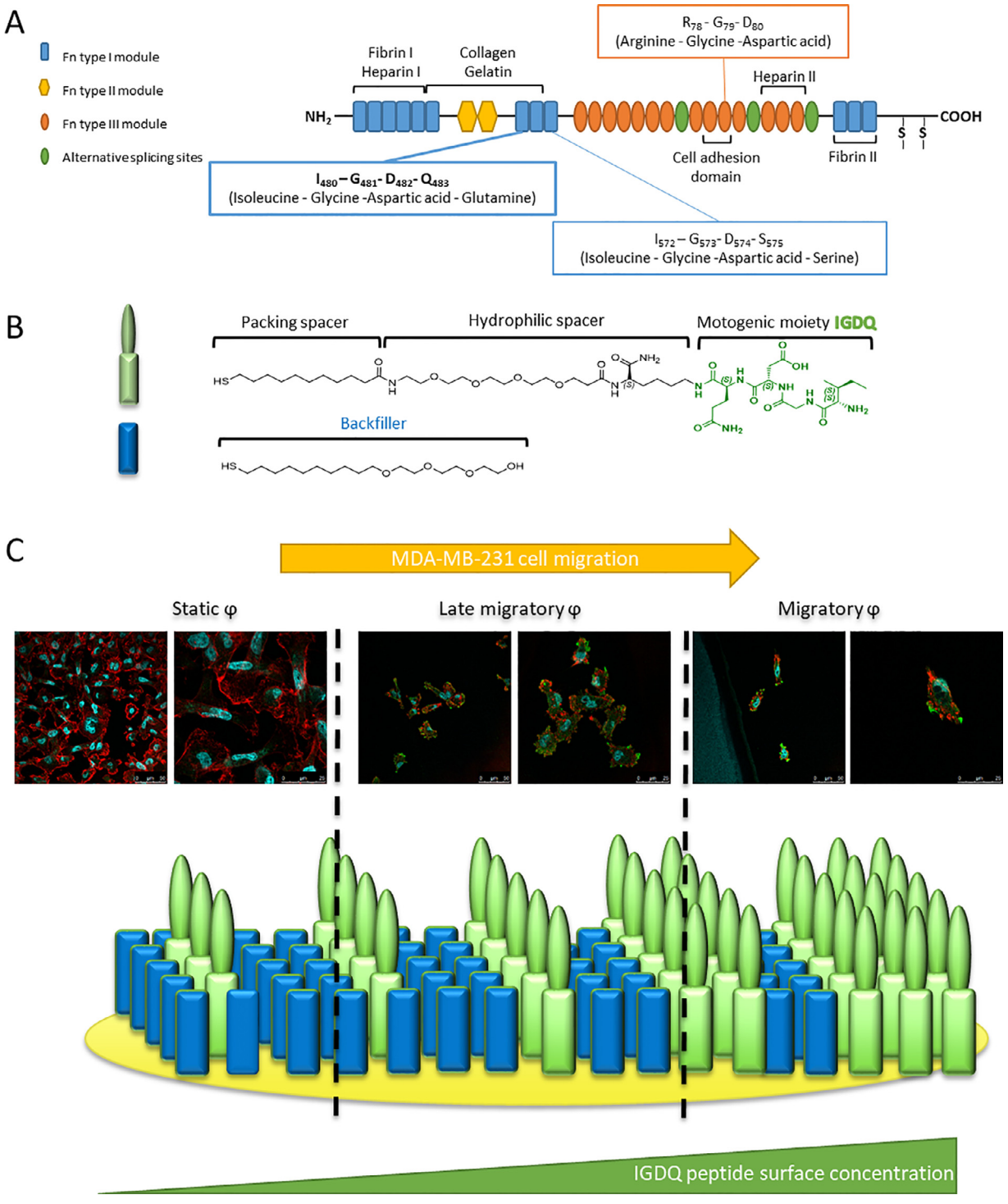

Fig. 1. Peptide-associated cell migration along engineered surfaces. A. Schematic representation of fibronectin and its functional motifs; B: Chemical structure of the peptides used for the gradient with the fibronectin motif IGDQ and the tetraethylenglycol as backfiller; C: Schematic representation of engineered surfaces after 5 days of cell migration; Immunofluorescent confocal microscopy images from control MDA-MB-231 cells (shCTL) labeled for ITGB3 (green), cytoskeleton (phalloidin – alpha-tubulin – red) and nucleus (Hoechst – UV / blue); ϕ: phenotype; static: proliferative cells; late migratory: cells which start migrating after day 3 of the experiment; migratory: cells which start migrating before day 3 of the experiment.

Integrin beta 3 and integrin alpha 5 are implicated in a wound healing assay

Collective migration was evaluated using a wound healing assay during 48h, with cell proliferation blockage (mitomycin C) (Figure 3). The control cells filled 87% of the wound in 48h while it was not the case for ITGA5 and ITGB3 knock-down cells for both shRNAs (Figure 3–A, Supplemental Figure 2E). shITGB3 cells were able to close only 22% of the scratch (Figure 3–B) and shITGA5 cells 33%, with a significant reduction of relative closing compared to shCTL cells (Figure 3–C). These results indicate that

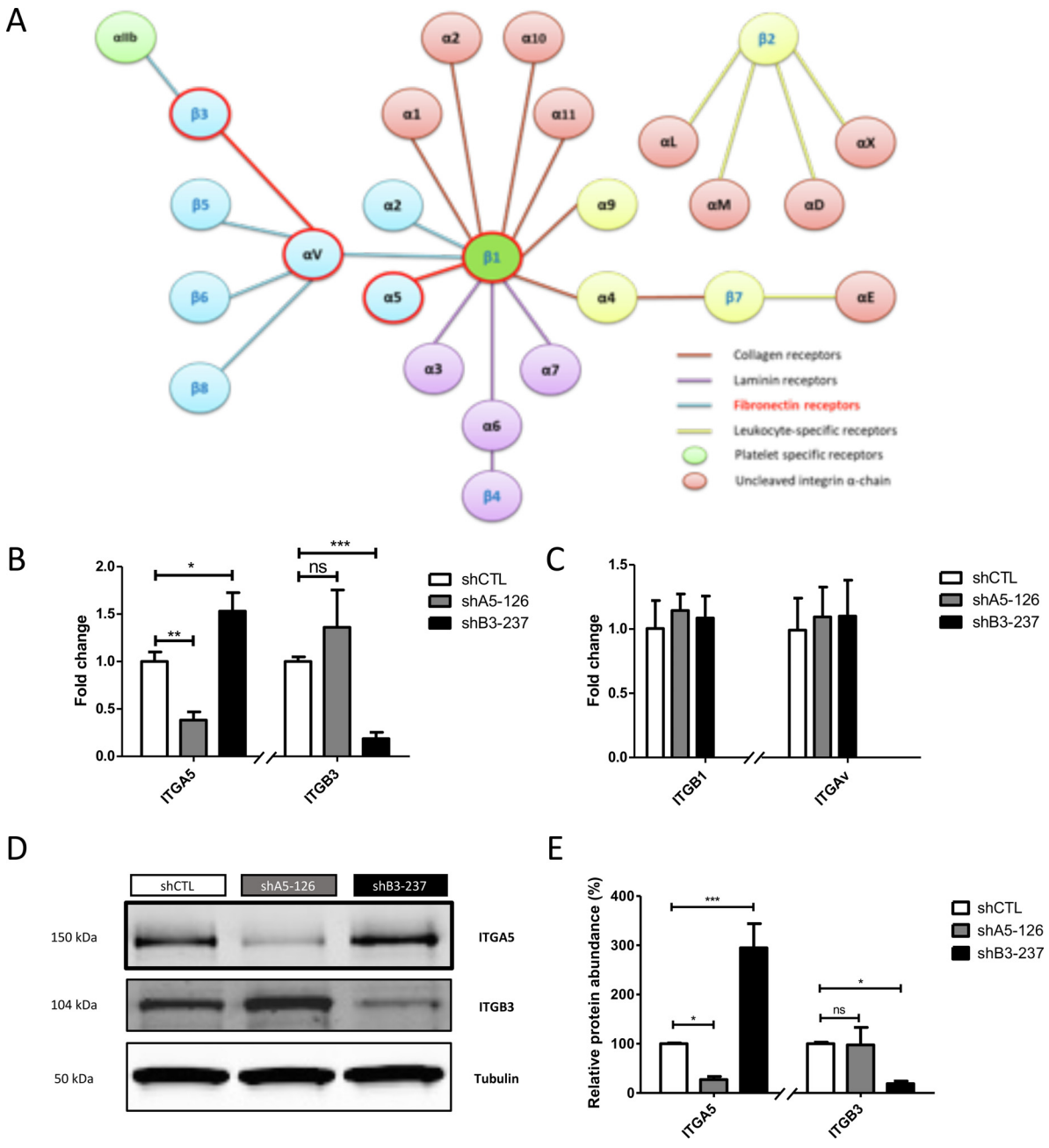

Fig. 2. Gene expression of alpha 5 (ITGA5) and beta 3 (ITGB3) integrins in small-hairpin RNA knock-down MDA-MB-231 cells. MDA-MB-231 cells were transfected using empty vector as control (shCTL), ITGA5-targeting (shA5-126) or ITGB3-targeting shRNA (shB3-237) lentiviral vector. A. Human integrin heterodimer combinations and their main ligand; B. mRNA levels of ITGA5 and ITGB3 were measured by RT-qPCR using α-tubulin as the house-keeping gene, results are expressed in fold change after being normalized to the control cells (shCTL); C. mRNA levels of ITGAv and ITGB1 were measured by RT-qPCR using α-tubulin as the house-keeping gene, results are expressed in fold change after being normalized to the control cells (shCTL); D: Representative western-blot for ITGA5, ITGB3 and α-tubulin; E: Quantification of protein abundance for ITGA5 and ITGB3 using α-tubulin as the loading control and shCTL as the control (mean $\pm$ 1 SD of three independent experiments); Statistical significance was determined by two-way ANOVA (*$p < 0.05$; **$p < 0.01$; ***$p < 0.001$).

ITGA5 and ITGB3 were needed for cell migration in a wound healing assay.

Integrin beta 3 and integrin alpha 5 are both necessary for IGDQ-mediated directional single cell migration

To investigate the role of ITGA5 and ITGB3 on IGDQ-mediated directional cell migration, cells were seeded on the motogenic surfaces (Figure 1) and the migration and proliferation of the cells were monitored by taking holographic images each day for 5 days (Figure 4).

Normal proliferation was observed in shCTL, shITGA5 and shITGB3 cells. Migrating shCTL cells were observed along the IGDQ gradient. However, no migrating cells were observed in both shITGA5 and shITGB3 cells, as shown by the quantification of the number of migrating cells in three independent experiments (Supplemental Figure 3). This was confirmed by using a second shRNA for ITGB3 (Supplemental Figure 4). This inhibition

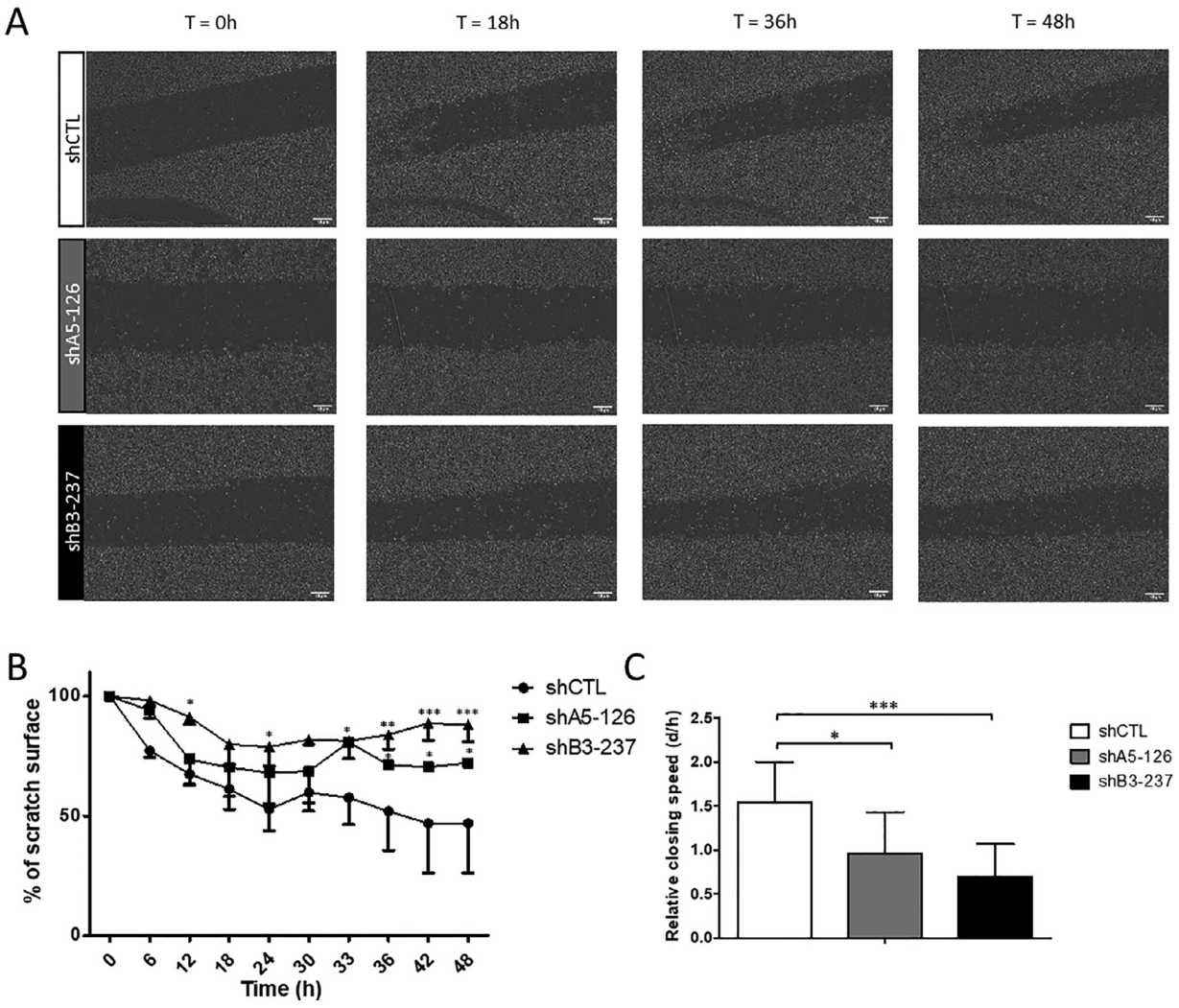

Fig. 3. Effects of shRNA knock-down for alpha 5 integrin (shA5-126) or for beta 3 integrin (shB3-237) on MDA-MB-231 cell migration on uncoated surface (post-transduction passage 14). A: *Cytonote* holographic wound healing time-lapse imaging for 48h on shCTL, shA5-126 or shB3-237 cell. B: Cell migration relative quantification assessed by imaging processing using *ImageJ* (macro *Phase Wound*) represented as the percentage of the whole scratch surface along time. Statistical significance was determined by two-way ANOVA (mean ± 1 SD of three independent experiments) ($^{*}p < 0.05$; $^{**}p < 0.01$; $^{***}p < 0.001$); C: Represented by cell relative speed (relative distance per hour calculated from the data of panel B), statistical significance was determined by unpaired t-test with Welch's correction (mean ± 1 SD of three independent experiments) ($^{*}p < 0.05$; $^{**}p < 0.01$; $^{***}p < 0.001$).

is statistically significant for both knock-down cell lines. The results showed that both ITGA5 and ITGB3 are necessary for the IGDQ-triggered single cell migration.

Integrin (αv)β3 is activated by IGDQ fibronectin type I motif

To investigate the integrin activation on IGDQ-exposing surfaces, shCTL, shITGA5 and shITGB3 cells were seeded on the surfaces for 5 days (Figure 1). The cells were seeded at day 1 where IGDQ peptide concentration is the lowest (Figure 1–A–B). Cells were incubated to permit their proliferation and migration during 5 days and we were able to obtain cells presenting three phenotypes: "static phenotype" for proliferating cells (low IGDQ concentration), "late migratory phenotype" and "migratory phenotype" for migratory cells that followed the IGDQ gradient concentration (Figure 1–C). At this step, cells were fixed and labeled for ITGA5 / F-actin (Figure 4–A–B–C, Supplemental Figure 5) or ITGB3 / F-actin (Figure 4–D–E–F, Supplemental Figure 6). When integrins are activated, focal adhesion complexes are observed at the plasma membrane.

In proliferating cells, no clusters were observed neither for ITGA5 nor for ITGB3 in any of the three cell lines. For both integrins, the labeling showed the presence of the protein at the plasma membrane, well distributed all over the surface of the cells as small dots (Figure 4). Migrating cells were observed only in shCTL cells. In these cells, ITGA5 labeling was observed all over the membrane as in proliferating cells (Figure 4–A). No clusters of ITGA5 were observed. This suggests that integrin α5(β1) was not activated by the IGDQ motif.

ITGB3 labeling in migrating cells showed large clusters at the membrane with a high density of ITGB3, corresponding to focal adhesion complexes due to integrin beta 3 activation (Figure 4–D). A light staining of ITGB3 at the rest of the membrane is also visible. This suggests that integrin (αv)β3 is activated by IGDQ fibronectin type I motif in cells with a migratory phenotype, but not in cells with a proliferative phenotype.

Integrin alpha 5 is activated by RGD type III fibronectin motif

To be sure that integrin alpha 5 kept its capacity to cluster in our model, wild type MDA-MB-231 (WT), shCTL or shITGB3 cells were seeded on

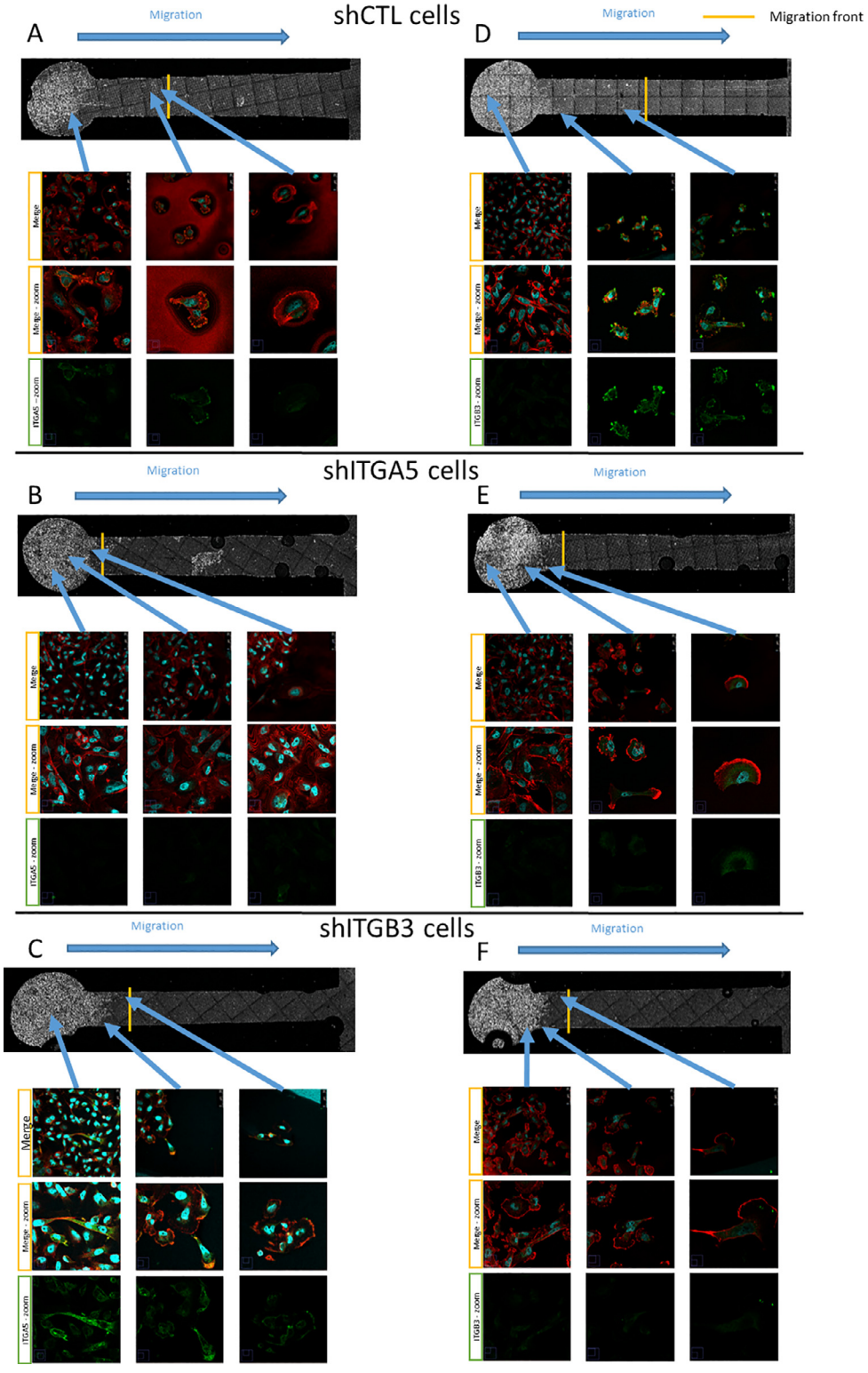

Fig. 4. Integrin knock-down MDA-MB-231 cells migrating on IGDQ-exposing surfaces (post-transduction passage 5): alpha 5 integrin (A, B, C) and beta 3 integrin subcellular localizations (D, E, F). Immunofluorescence labeling of alpha 5 integrin (ITGA5 - green), cytoskeleton (phalloidin – alpha-tubulin – red) and nucleus (Hoechst – UV / blue) A: Control cells (shCTL); B: Cells knock-down for alpha 5 integrin (shA5-126); C: Cells knock-down for beta 3 integrin (shB3-237). The black round dots correspond to air bubles. Immunofluorescence labeling of beta 3 integrin (ITGB3 - green), cytoskeleton (phalloidin – alpha-tubulin – red) and nucleus (Hoechst – UV / blue) D: Control cells (shCTL); E: Cells knock-down for alpha 5 integrin (shA5-126); F: Cells knock-down for beta 3 integrin (shB3-237). The black round dots correspond to air bubles. A x200% zoom was applied for "Merge – zoom" and "ITGA5 or ITGB3 – zoom". These images are representative of 3 independent experiments each performed with 3 technical replicates, performed at different passages post-transduction.

classical culture plates or on high concentration fibronectin coated surfaces. On these surfaces, fibronectin exposes the RGD motif. The labeling of ITGA5 was performed 48 hours later (Figure 5).

On classical culture plates, ITGA5 labeling was observed all over the plasma membrane as observed on engineered surfaces, for both shCTL and shIGTB3 cells (Figure 5–A–C). On Fn type III coated surfaces in WT cells, ITGA5 staining showed cross-bars, perpendicularly to the membrane (Figure 5–B–D). This is due to integrin alpha 5 activation and clustering. Small dots of ITGA5, with a light staining, are also visible on the whole membrane surface. These results indicate that ITGA5 is activated by high concentrations of Fn type III, containing RGD motifs. Moreover, the ITGA5 clustering is not affected in shCTL cells, neither by the absence of ITGB3 (Figure 5 D).

In parallel, ITGB3 staining also performed on WT cells. On both uncoated and Fn type III coated surfaces, ITGB3 staining showed the homogenous presence of the protein at the membrane appearing as small dots (Figure 5–E–F). This suggests that integrin (αv)$\beta 3$ is not activated by high Fn type III module that contains the RGD motifs.

Co-regulation of recycling transport of integrin beta 3 by integrin alpha 5 is potentially necessary for directional IGDQ-mediated cell migration

To deepen the investigation and to understand the interactions between ITGA5 and ITGB3, a whole proteomic analysis was performed in ITGA5 and ITGB3 knock-down cells according to the workflow presented in Supplemental Figure 7. Then for each experiment, proteins significantly differentially expressed were analyzed in a unsupervised hierarchical comparative gene ontology analysis to identify the ones that are enriched. Gene ontology is a bioinformatics tool that permits to cluster genes or proteins under a term, this term describing either a biological process (pathways), a molecular function (protein binding) or a cellular component (protein localization). Gene ontology clusters significantly enriched (FDR $>$ 0.1) were then clustered using *ClueGo* (Cytoscape tool, consulted on 2020-01). In this study, we choose to globally integrate all significant proteins into cellular processes or subcellular localization clusters. We performed gene ontology (GO) enrichment analysis of the identified differentially expressed proteins to gain insights into the cellular functions and biological processes that are affected by integrin alpha 5 or integrin beta 3.

For each comparison, shCTL vs shITGA5 and shCTL vs shITGB3, the number of proteins detected (Supplemental figure 8–A–C), volcano plot representing the repartition of proteins expressed obtained from quantitative proteomics analysis where green dots represent proteins exhibiting significant fold changes (Supplemental figure 8–B–D), top 10 dysregulated proteins (Figure 6–7–A), top 10 upregulated (Figure 6–7–B) and top 10 downregulated proteins (Figures 6–7–C), the top 15 gene ontology categories impacted according to the percentage of their dysregulated proteins (Figures 6–7–D), the gene ontology categories (GO) impacted by the knock-down (ClueGo trees - Figures 6–7–E) and the repartition of major enriched gene ontology clusters for biological processes (Figures 6–7–F) or for cellular localization (Figures 6–7–G) were obtained using bioinformatics analysis (Figures 6–7). About 2500 proteins were identified in each experiment, with 142 proteins significantly dysregulated in shITGA5 cells and 245 in shITGB3 cells compared to shCTL cells (Supplemental Table 1). It is interesting to notice that the list of the top dysregulated proteins (Figures 6–7–A–B–C) and the list of the top gene ontology categories impacted (Figures 6–7–C) do not always reflect the global impact of the knock-down. Indeed, the main dysregulated proteins are perhaps not the most interesting to study, while the panorama allows to focus both on a specific pathway and related proteins, at the level of biological processes (Figures 6–7–E–F) and cell localization (Figures 6–7–G).

Integrin alpha 5 is linked to vesicle-mediated transport

The invalidation of ITGA5 induced modifications in the expression of proteins involved in multiple biological processes (Figure 6–D–E–F–G; Supplemental table 2). Our analyses revealed in that GO categories and hub proteins significantly enriched were linked to vesicle-mediated transport regulation, catabolic processes, nucleoplasmic transport, cell-substrate junction and cell isolation stress. Interestingly, two GO category clusters impacted by ITGA5 knock-down are similarly ranked in the top 4 modified biological processes (Figure 6–F) and top 2 modified subcellular localizations GO categories (Figure 6–G). This two GO clusters are: endoplasmic reticulum – Golgi apparatus and catabolic process, the latter including proteasome complex, positive regulation of cellular catabolic process and protein deubiquitination.

First, around one-fourth of biological processes and one-third of protein cellular localization GO categories are associated endoplasmic reticulum (ER) to Golgi-vesicle mediated transport (Figure 6 D–E–F). Moreover, "vesicle cargo loading" appears in the top 15 impacted GO categories (Figure 6–D). It is also represented by top downregulated proteins such as the calcium binding protein PDCD6, the GTPase-activating protein ArfGAP3 and the glycogen debrancher enzyme AGL ("Golgi to endoplasmic reticulum retrograde transport regulation Ca^{2+} dependent signaling pathway") and top upregulated protein like the valosin-containing protein (VCP)-interacting molecule ANKRD13A (lysosomal trafficking) (Figure 6–A to C). This suggest the involvement of ITGA5 in vesicle-mediated transport regulation.

Second, ITGA5 knock-down cells was also enriched with one-fourth biological processes and one-third protein cellular localization GO categories linked to the catabolic processes at mRNA and protein levels (Figure 6–E–F–G). Moreover, multiple GO categories linked to this hub appears in the top 15 impacted GO categories including "regulation of RNA binding" and "pre-mRNA cleavage required for polyadenylation" (Figure 6–D). It is represented by top downregulated proteins such as the nucleotide excision repair protein RAD23A (proteasome complex), the aminoacyl-tRNA synthase complex auxiliary component EEF1E1 (translation regulation) and the kinase PIK3C2A (endosomal maturation and autophagy).

Third, around one-seventh of biological processes and one-ninth of protein cellular localization GO categories are related to cytoskeleton regulation GO's hub. This hub includes cell-substrate junction assembly, response to isolation stress (linked to cell detachment from other cells like in single cell migration), integrin complex and adherents junctions (Figure 6–E–F–G). Moreover, "response to isolation stress", "cell adhesion mediated by integrins" and "cell-substrate junction assembly" appears in the top 15 impacted GO categories (Figure 6–D). It is also represented by top downregulated proteins such as the estrogen resistance protein BCAR3 (cell motility promotion, adhesion remodeling and cytoskeleton reorganization), the nucleotide excision repair protein (reduced characteristics of stemness-EMT) and the apoptotic suppressor proteins XIAP (pro-metastatic phenotype), and top upregulated protein like the cell motility mediator MEMO1 (lamellipodial actin network, adhesion site formation and microtubule outgrowth in cell motility) (Figure 6–A to C). Altogether, this suggests that ITGA5 has a role in cytoskeleton component modulation.

Fourth, ITGA5 knock-down cells were also enriched with one-fourth biological processes and 4% protein cellular localization GO categories, linked to nucleoplasmic transport (Figure 6–E–F–G). In the top upregulated proteins, was ranked the nucleoporin NUP37.

Integrin beta 3 linked to protein expression and metastatic cell capacity

The invalidation of ITGB3 induced modifications in the expression of proteins involved in multiple biological processes (Figure 7–D–E–F–G; Supplemental table 2). Our analyses revealed in ITGB3 knock-down cells GO categories and hub proteins significantly enriched were linked to EMT, mRNA splicing and catabolism, protein production. Interestingly, the two major GO hubs RNA modifications and protein translation represent more

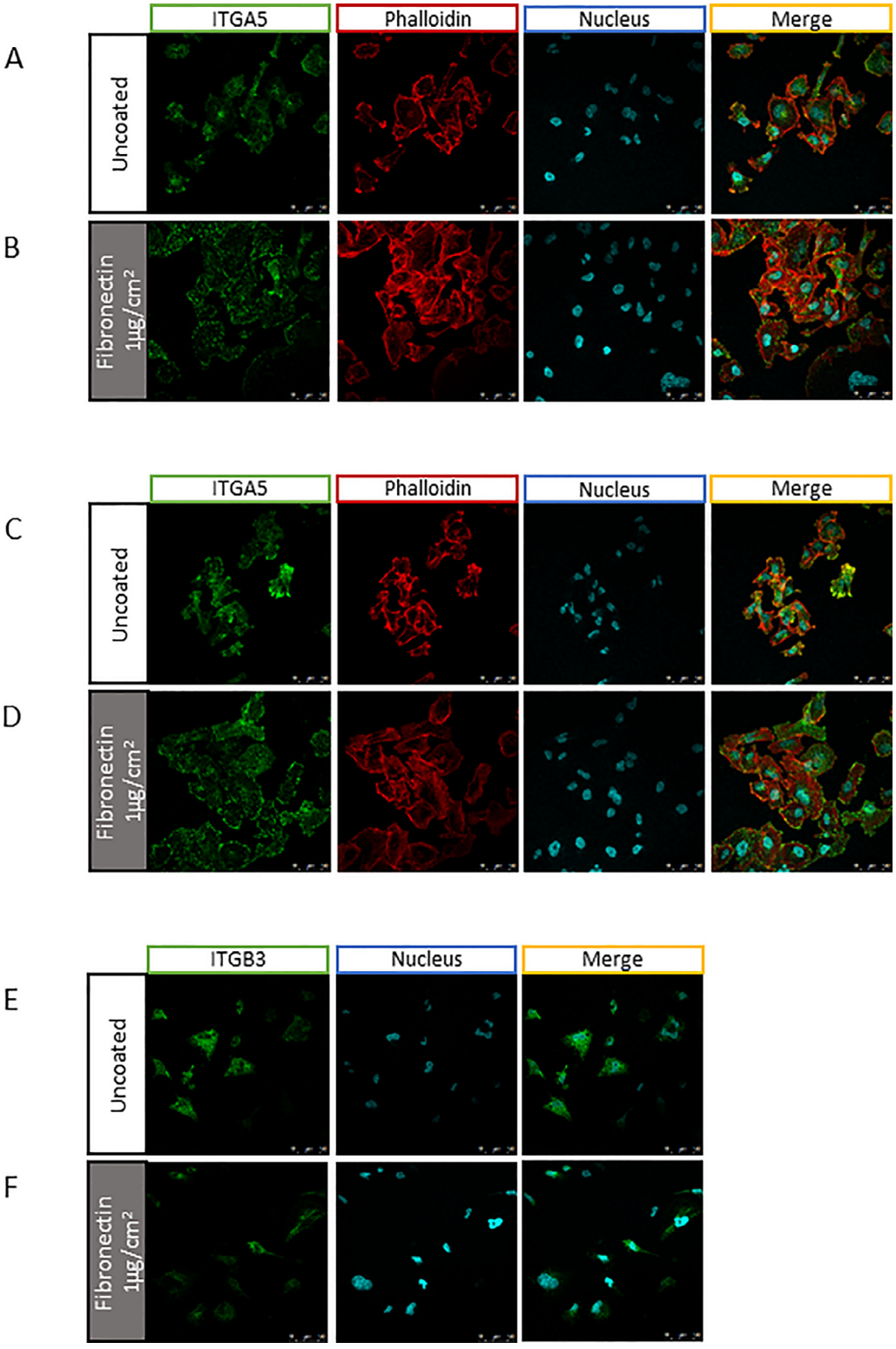

Fig. 5. Effect of fibronectin coating on alpha 5 and beta 3 integrin abundance and subcellular localization. Immunofluorescence labeling of alpha 5 integrin (ITGA5 - green), cytoskeleton (phalloidin – alpha-tubulin – red) and nucleus (Hoechst – UV) in control cells (shCTL): A. Uncoated surface; B. Surfaces coated with fibronectin at 1 µg/cm^2. Immunofluorescence labeling of alpha 5 integrin (ITGA5 - green), cytoskeleton (phalloidin – alpha-tubulin – red) and nucleus (Hoechst – UV) in cells knock-down for beta 3 integrin (shB3-237): C. Uncoated surface; D. Surfaces coated with fibronectin at 1 µg/cm^2. Immunofluorescence labeling of beta 3 integrin (ITGB3 – green) and nucleus (Hoechst – UV) in wild type cells (WT): E. Uncoated surface; F. Surfaces coated with fibronectin at 1 µg/cm^2.

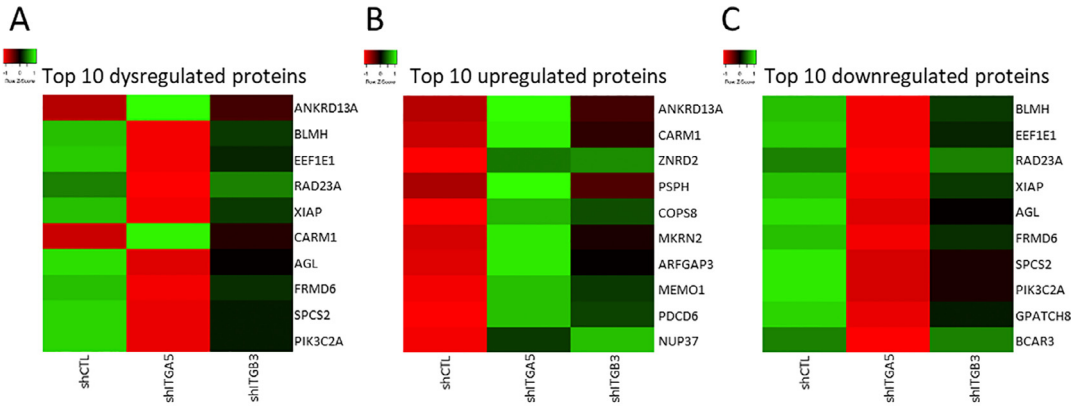

D

GO terms - shITGA5	GO	% impacted proteins
meiotic chromosome condensation	GO:0010032	40
common-partner SMAD protein phosphorylation	GO:0007182	33
response to isolation stress	GO:0035900	33
peptidyl-arginine methylation, to asymmetrical-dimethyl arginine	GO:0019919	29
hemidesmosome assembly	GO:0031581	25
pre-mRNA cleavage required for polyadenylation	GO:0098789	25
regulation of RNA binding	GO:1905214	25
positive regulation of transcription by RNA polymerase I	GO:0045943	18
cell adhesion mediated by integrin	GO:0033627	18
vesicle cargo loading	GO:0035459	18

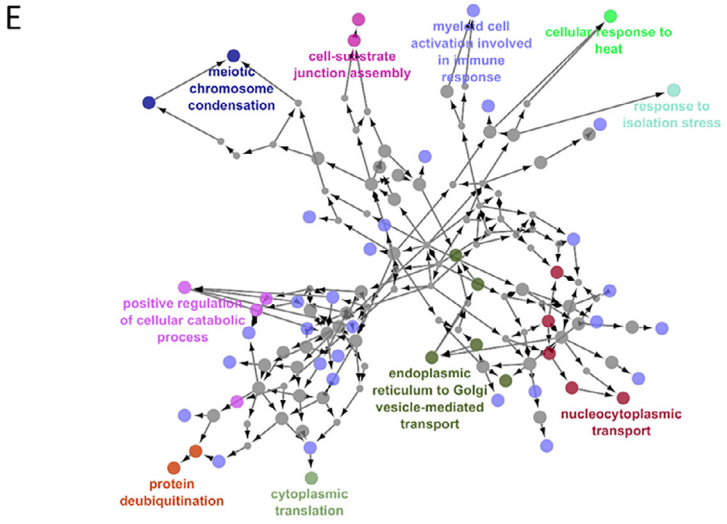

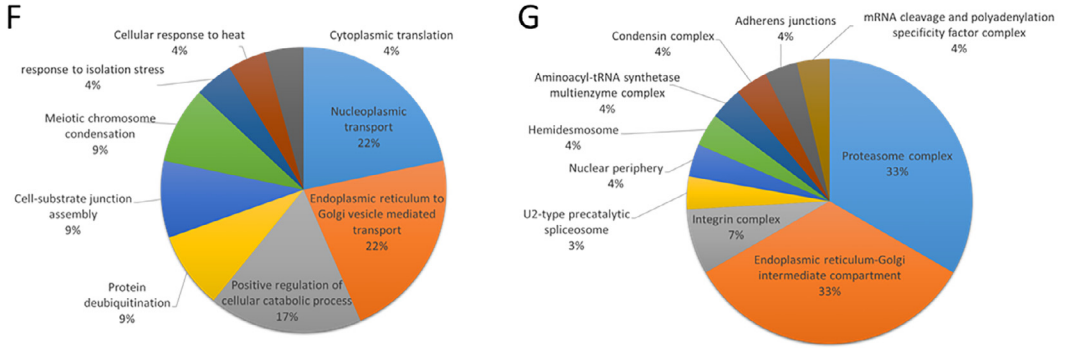

Fig. 6. Relative differential protein expression analysis for alpha 5 integrin knock-down cells. Raw data from mass spectrometry were processed to obtain protein differential expression in shA5-126 knock-down cells compared to control cells (shCTL) using total spectral counting and t-test with p-value < 0.05. A: Top 10 differentially expressed proteins; B: Top 10 upregulated proteins; C: Top 10 downregulated proteins;; D: Top 10 relevant gene onthology categories (GO) - biological processes (BP) modified ranked according to percentage of proteins dysregulated in GO category considered; E: String map of more relevant gene onthology categories (GO) - biological processes (BP) modified (p-value < 0.1, *STRING, Cytoscape-GoClue*); F: Major gene ontology - biological process clusters modified; G: Major gene ontology – cellular component clusters modified.

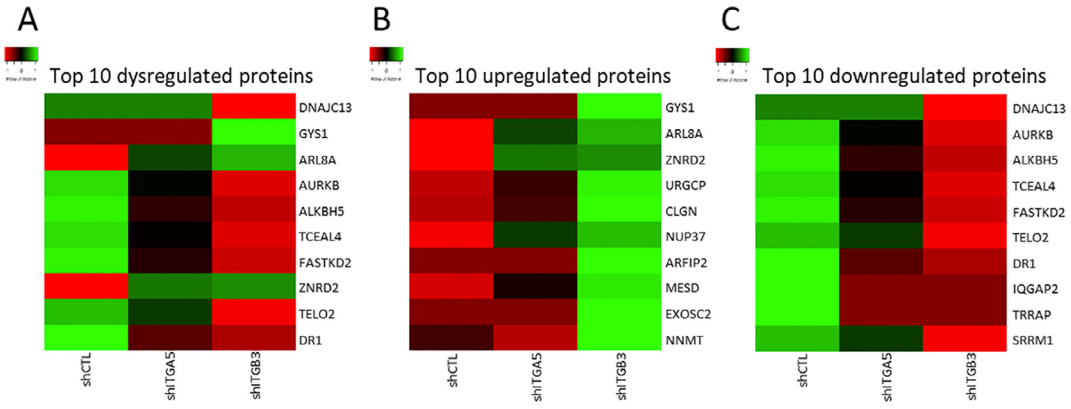

D

GO terms - shITGB3	GO	% impacted proteins
progesterone receptor signaling pathway	GO:0050847	25
regulation of deoxyribonuclease activity	GO:0032070	20
spindle elongation	GO:0051231	18
cleavage involved in rRNA processing	GO:0000469	13
ribosomal large subunit assembly	GO:0000027	10
binding of sperm to zona pellucida	GO:0007339	9
maturation of SSU-rRNA from tricistronic rRNA transcript (SSU-rRNA, 5.8S rRNA, LSU-rRNA)	GO:0000462	8
positive regulation of telomere maintenance via telomere lengthening	GO:1904358	8
maturation of SSU-rRNA	GO:0030490	8
ribosomal large subunit biogenesis	GO:0042273	6

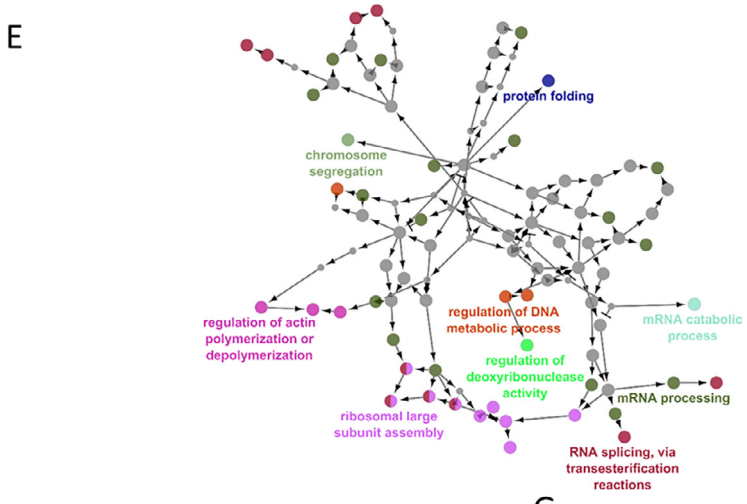

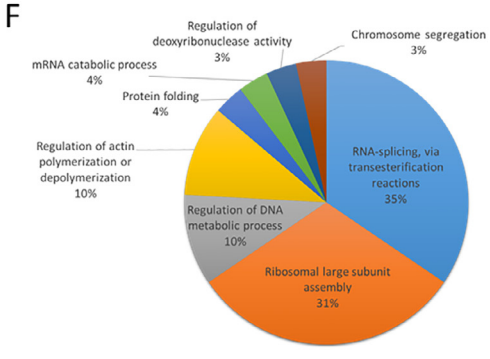

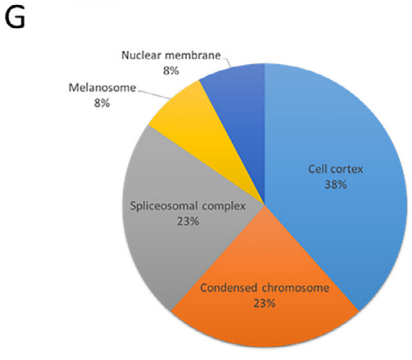

Fig. 7. Relative differential protein expression analysis for beta 3 integrin knock-down cells. Raw data from mass spectrometry were processed to obtain protein differential expression in shB3-237 knock-down cells compared to control cells (shCTL) using total spectral counting and t-test with p-value < 0.05. A: Top 10 differentially expressed proteins; B: Top 10 upregulated proteins; C: Top 10 downregulated proteins;; D: Top 10 relevant gene onthology categories (GO) - biological processes (BP) modified ranked according to percentage of proteins dysregulated in GO category considered; E: String map of more relevant gene onthology categories (GO) - biological processes (BP) modified (p-value < 0.1, *STRING, Cytoscape-GoClue*); F: Major gene ontology - biological process clusters modified; G: Major gene ontology – cellular component clusters modified.

than four-fifth of biological processes and half of protein cellular localization (Figure 7–E–F–G).

First, ITGB3 knock-down cells was enriched with two-fifth biological processes and one-fourth protein cellular localization GO categories linked to RNA modifications and metabolism (Figure 7–E–F–G). Moreover, multiple GO categories linked to this hub appear in the top 15 impacted GO categories including "cleavage involved in rRNA processing", maturation of SSU-rRNA and RNA splicing. (Figure 7–D). The splicing factor SRRM1 (modifications in splicing of RNA) was found in the top downregulated proteins (Figures 7–A to C). This supports the involvement of ITGB3 in RNA regulation and maturation.

Second, around two-fifth of biological processes and one-fourth of protein cellular localization GO categories are associated to protein metabolism (Figure 7–D–E–F). Moreover, multiple GO categories linked to this hub appear in the top 15 impacted GO categories including ribosomal large subunit assembly and biogenesis (Figure 7–D). It is represented by top upregulated proteins such as the chaperone proteins CLGN and MESD (protein folding) (Figure 7–A to C). This supports the involvement of ITGB3 in protein translation and metabolism.

Third, around one-tenth of biological processes and two-fifth of protein cellular localization GO categories are associated to cytoskeleton organization (Figures 7–D–E–F). Indeed, cell cortex localization is the region beneath the plasma membrane that contains a network of actin filaments and associated proteins. In this hub, all GO categories related to cell motility and stemness are included. Top upregulated proteins such as the GTPase activating protein IQGAP2 (cell contractile regulation and invasiveness inhibition), the kinase TRRAP (stemness) and the demethylase ALKBH5 (invasiveness promotion) and top upregulated proteins like the methyltransferase NNMT (EMT regulation) are linked to these categories (Figures 7–A to C).

Fourth, around one-tenth of protein cellular localization GO categories are associated to melanosome, which is a vesicle that contains melanin in melanocytes (Figure 7–F). Top upregulated proteins such as the heat-shock co-chaperone DNAJC13 endosomal trafficking regulation) and top upregulated proteins like the GTPase ARL8B (lysosomal transport) and the exosome component EXOSC2 (exosome regulation) are included in this category (Figure 7–A to C). This suggests an implication of ITGB3 in the trafficking of multiple vesicle types.

We also analyzed if there were common differentially expressed proteins found in shITGA5 cells and in shITGB3 cells as compared to shCTL cells (Supplemental table 2). Eighteen proteins were identified of whose 17 were similarly up-regulated or down-regulated in both cell lines.

Discussion

Integrins are major players of metastatic process. In this work, we focused on cancer cell migration and we studied the role of alpha 5 and beta 3 integrin subunits. Both integrins are described to be activated by fibronectin. In previous other studies, using siRNA or shRNA knock-down, it was shown that both integrins are implied in cell migration. ITGB3 is described to be linked to directional cell migration [33] and ITGA5 to random cell migration. Cell migration is regulated by ECM elements either in tissues or on artificial coated surfaces. Indeed, ITGA5 was described to be implied in regulating random cell migration on high-fibronectin coated surfaces while ITGB3 is implied in directional migration on low-fibronectin coated surfaces [34]. Except in studies on embryo development or on integrin trafficking, all other works studied these integrins separately regarding their impact on cell migration. In this work, we studied in parallel the impact of both integrins $\alpha v\beta 3$ and $\alpha 5\beta 1$ in a triple breast cancer cells in *in vitro* model, and more specifically regarding their implication in IGDQ-mediated cell migration. To achieve this objective, we knocked down each one of the two subunits using shRNA. The collective migration was evaluated using a wound healing assay on uncoated surfaces and single cell migration performed on the surface exposing an IGDQ gradient. A complementary full proteomic analysis was performed to determine the interplay between both integrins and their role in cancer cell migration. Using bioinformatics analyses, an overview of the potential roles of the integrins of interest has been unraveled. An experimental validation will be necessary to confirm this hypothesis.

In this study, we showed that ITGB3 and ITGA5 are necessary for cell migration in a wound healing assay. Moreover, we discovered that ITGB3 expression induced a negative control on ITGA5 expression at mRNA and protein levels. To the best of our knowledge, no previous study demonstrated a mutual regulation between beta 3 and alpha 5 integrin expression. This might be explained by a compensation system due to the loss of ITGB3, while the reverse is not true, i.e. alpha 5 integrin does not seem to influence integrin beta 3 expression. The study of miRNAs can be a good path to explain for the overexpression of ITGA5 observed in integrin beta 3 knock-down cells.

The motogenic effect of IGD(Q) motif from fibronectin type I module was first described in 1999 by Schor & al. [19], showing an activation of fibroblast migration using soluble IGD peptides. This activity depends on functional integrin $\alpha v\beta 3$, the phosphorylation of FAK at the tyrosine position 125 and the inhibition of $\alpha 5\beta 1$ mediated signaling. Moreover, IGDQ was linked only to cell migration and not to cell adhesion onto Fn [35], unlike RGD motif fibronectin type III module [36]. Our results showed that IGDQ fibronectin type I motif activates ITGB3 during single cell migration and not during cell proliferation while ITGA5 clustering is induced by Fn type III containing RGD motif. Interestingly, the absence of ITGA5 induced the loss of cell migration capacity on IGDQ-exposing surfaces, despite the fact that ITGB3 is expressed and localized at the cell membrane. It was previously shown that the transduction cascade following the IGDQ exposure to fibroblast is inhibited by signaling mediated through integrin $\alpha 5\beta 1$. Coupled with our results, this suggests a necessity to have this $\alpha 5\beta 1$ and $\alpha v\beta 3$ signaling co-regulation to permits the IGDQ-mediated cell migration. It has to be noted that RhoA and Rac1 protein abundance was not affected by ITGA5 or ITGB3 knock-down (data not shown), indicating that the modification observed in cell migration was not due to a change in the expression of these two proteins.

Our proteomic results also pointed out a modification in RNA translation, splicing and metabolism in shITGB3 cells. Links between RNA translation and focal adhesion complexes formed by integrins activation were already described since 20 years. Chicurel & al. [37] showed the localization of ribosomal complexes near focal adhesion complexes, suggesting a new type of gene regulation by integrins and by mechanical stress. The spatial localization of translation facilitate local protein enrichment at their sites of function. This permits to have a physical proximity of translated proteins and their binding partners. The co-localization / compartmentalization of translation related proteins (ribosomes, EIF4E - EIFE4G), microtubules, microfilaments and focal adhesion (vimentin) at the lamelipodia of migrating fibroblasts was evidenced by Willett & al. [38]. These data showed a direct link between cell migration and this focal adhesion/integrin-mediated translation. The same team demonstrated a preferential association between integrin beta 3 and 40S ribosomal subunits, all along the lamelipodia in migrating fibroblasts [39]. In our integrin beta 3 knock-down model, EIF5B (Eukaryotic translation initiation factor 5B), one of the proteins necessary for the translation initiation was found downregulated with 0.8 fold-change (p-value: 0.0044). Interestingly, EIF5B binds to EIF4E and can be connected to ITGB3 via the mTOR-EGFR pathway. This suggests a potential integrin-mediated translation dependent of ITGB3 and EIF5B.

The loss of migration capacity on IGDQ-exposing surface can be linked to a defect of ITGB3 clusterisation in ITGA5 knock-down cells, which is dependent on integrin recycling trafficking. These results, added to the results of our proteomic analysis, suggest that ITGA5 regulates ITGB3 trafficking, more specifically the recycling one, that allows to form ITGB3 clusters after its activation. Moreover, ITGB3 is found at the membrane indicating that the membrane addressing is not modified. On the other

hand, the reverse compensating regulation was not observed (Figure 5). Indeed, the loss of ITGB3 did not modify ITGA5 clustering upon $\alpha5(\beta1)$ activation on Fn coated surfaces (RGD motif). It has been shown that the recycling transport of $\alpha5\beta1$ and $\alpha v\beta3$ is co-dependent. The transport of $\alpha5\beta1$ inhibits the transport $\alpha v\beta3$ and reciprocally. But from our knowledge, no study indicates this potential necessary presence of $\alpha5\beta1$ to allow the $\alpha v\beta3$ recycling transport [34]. It was shown that $\alpha v\beta3$ blockage in rich-fibronectin environment promotes $\alpha5\beta1$ dependent random cell migration via filopodia. At the same time $\alpha v\beta3$ activation inhibits $\alpha5\beta1$-dependent cell migration and induces directional migration in low-fibronectin environment [40]. All those processes are Rab-dependent and also implied the lysosomal regulation and trafficking [41–45]. It would be interesting to study the trafficking of both integrins during cell migration on IGDQ-exposing surfaces. Furthermore, since this study has been performed using MDA-MB-231 cells, it would also be interesting to study other cell lines, with different in vitro migration properties and/or different metastatic capacities when injected in vivo.

The trafficking of integrins was described, at different levels, as essential for cellular migration [46] and cancer metastasis promotion [47]. Indeed, it was shown that exosome containing integrins are implied in cell migration through a crosstalk with stromal fibroblast cells, but also in organotropy where exosomes containing $\alpha6\beta4$ and $\alpha6\beta1$ were linked to lung metastasis, while exosomes containing integrin $\alpha v\beta5$ were linked to liver metastasis [48]. Furthermore, the endocytosis of integrins, permitting their recycling, plays a major role in cell migration [49]. Using surface gradients allowed to highlight the mechanisms involved in integrins trafficking in cell migration triggered by IGDQ and, in the future, will help to highlight potential targets to prevent metastasis in cancer patients.

Materials and methods

Reagents

All the reagents and their references are described in Supplementary Table 2.

Cell culture

The metastatic breast cancer MDA-MB-231 cell line (pleural effusion – woman 51 year old - ATCC® HTB-26™) was cultivated in RPMI-1640 medium containing L-glutamate (Gibco) supplemented with 10% fetal bovine serum (Gibco). HEK293 lung cancer cell line (ATCC) was cultivated in DMEM – low glucose (Gibco) supplemented with 10 % fetal bovine serum (Gibco) and 1 % glutamine. Cells were grown in a humidified atmosphere at 37°C with 5 % CO_2 and are regularly checked to be mycoplasm-free

shRNA containing vector bacterial amplification

Bacterial amplification was performed with transformed competent bacterial glycerol stock containing sequence of the shRNA ITGA5-targeting (shA5-126 – CCGGGATGCA GTGAATTGTA CCTATCTCGA GATAGGTACA ATTCACTGCA TCTTTTT) or shRNA ITGB3-targeting (shB3-237 – CCGGAGGCAG ATCCAGGACT ATATTCTCGA GAATATAGTC CTGGATCTGC CTTTTTTG), ampicillin resistance for prokaryote selection and puromycin resistance for eukaryote selection in a SHC001 vector (MISSION shRNA – Sigma Aldrich). A starter amplification was prepared in 5 mL sterilized lysogeny broth (LB) medium with 20 µL of glycerol stock and 5 µL of ampicillin at 50 mg/mL (Roche) for 8 hours at 37°C - 125 rpm shake. The bacterial starter was then transferred into 125 mL of sterilized LB medium and 125 µL of ampicillin 50 mg/mL for 12 hours at 37°C – 125 rpm shake. The purification of plasmids was performed using the *Plasmid Plus Maxi kit* (Qiagen) following the manufacturer instructions for *high-copy plasmid*. Quality and concentration were determined using *Nanodrop N-100* spectrophotometer (Isogen Life Science) by measuring the absorbance at 230 and 260 nm. Samples were stored at -20°C.

Lentiviral particle production

Transient co-transfection of HEK293T cells was used to produce the lentiviral particles containing the empty vector (SHCOO1 – shCTL), the shRNA ITGA5-targeting vector or the shRNA ITGB3-targeting vector. The co-transfection was performed using three vectors. A mix containing 3.34 μg of Δ8.3 vector (pol), 1.67 μg of VSV-G vector (env) and 5 μg of lentiviral vector in the diluent (720 μL ddH_2O, 110 μL $CaCl_2$ 2.5 M) was mixed dropwise with 840 μL HeBS 2X (274 mM NaCl, 10 nM KCl, 1.5 mM Na_2HPO_4, 1 g dextrose, 50 mM Hepes) and incubated at room temperature for 20 min. The mix was added to half confluent HEK293T cells in DMEM medium supplemented with 10% fetal bovine serum and 1 % glutamine. The transfection medium was removed and replaced by fresh medium 24h post-transfection. At 48h post-transfection, lentivirus-containing supernatant was harvested and used directly for the following experiments.

Short-hairpin RNA knock-down (shRNA)

In T25 culture flask (Corning), 0.3 * 10^6 MDA-MB-231 cells were seeded 24h before the transduction to have one flask for: selection control (no transduction - selection), untransduced cells (no transduction – no selection), shCTL, shA5-126 and shB3-237. The supernatant containing the lentiviral particles was centrifuged and diluted 1/5 in RPMI-1640 medium containing L-glutamate supplemented with 10% fetal bovine serum. The diluted lentiviral particles complemented with transducing agent (protamine sulfate – 0.06 mg/mL) was droped on the prepared MDA-MB-231 cells for 48h hours. The medium was then replaced by fresh complete medium containing puromycin (2 µg/mL – Sigma-Aldrich) to select transduced cells. The selection was maintained during the following experiments.

RNA extraction

MDA-MB-231 cells grown in T25 flask (0.4 * 10^6 cells for 48h) were washed with PBS (20 mL phosphate buffer - KH_2PO_4 0.5 mM at pH 7.4, 9g NaCl qsp 1L bidistilled water) on ice, scraped off the plastic surface in PBS, centrifuged in 1.5 mL Eppendorf tube at 1000 rpm – 4°C and cell pellet harvested with 600 µL of RLT Lysis Buffer from *RNeasy Mini Kit* (Qiagen) in a 2 mL tube. Total RNA was extracted using the RNeasy Mini Kit and the automate *QIAcube* (Qiagen, Germany) under conditions "Large sample with DNase" and an elution volume of 30 μL. Total RNA concentration and quality were evaluated using *Nanodrop* N-100 spectrophotometer (*Isogen Life Science*) by measuring the absorbance at 260 nm and 230 nm. The samples were kept at -80°C.

Reverse transcription-quantitative PCR

Complementary DNA (cDNA) synthesis was performed from total RNA using *GoScript reverse transcription kit* (Promega), following the manufacturer instructions. 1 μg of total RNA was diluted with RNase-free water up to 12 μL. The samples were incubated at 70°C for 5 minutes. A reaction mix containing 4 μL of GoScript buffer mix with random primers, 2 μL of GoScript enzyme mix and 2 μL of nuclease-free water was added to each sample. The samples went under a temperature profile of 5 minutes at 25°C, 60 minutes at 42°C and 15 minutes at 70°C. The cDNA sample tubes were stored at -20°C.

Quantitative PCR (qPCR) was performed on a ViiA7 Real-Time PCR System (Thermo Fisher Scientific) using GoTaq® qPCR kit (Promega). A qPCR mix was prepared with 5.56 μL of MilliQ water, 0.22 μL of each

forward and reverse primer (Integrated DNA Technologies) to 300 nM (Supplemental Table 2) and 10 μL GoTaq® qPCR Master Mix (Promega). 4 μL of 1/100 diluted cDNA and 16 μL of the reaction mix per well were added in a qPCR 96-well reaction plate (Thermo Fisher Scientific) and the plate was sealed and centrifuged at 600 rpm for 1 minute. The temperature profile was 95°C for 2 min followed by 40 cycles of amplification at 95°C for 5 s, 60°C for 20 s, and 70°C for 20 s and a melting curve analysis at 65°C to 95°C with 0.5°C per 5 s increments. The amplification was quantified using the threshold cycle (Ct) method using ViiA 7 Real-Time PCR software (Thermo Fisher Scientific).

Gene expression was determined using the ΔΔCt method with tubulin as the housekeeping gene and shCTL as the reference sample as followed:

$$\begin{aligned} \mathbf{\Delta}Ct &= Ct\ gene\ of\ interest - Ct\ reference\ gene \\ \mathbf{\Delta\Delta}Ct &= \Delta Ct\ of\ the\ gene\ in\ condition\ of\ interest \\ &\quad - \Delta Ct\ of\ \ the\ gene\ in\ the\ control\ condition \\ \mathbf{Foldchange} &= 2^{(-\Delta\Delta Ct)} = relative\ gene\ expression\ compared\ to\ the\ control\ condition \end{aligned}$$

Protein extraction

MDA-MB-231 cells grown in T25 flask (0.4 * 10^6 cells for 48h) were washed with PBS on ice, scraped off the plastic surface in PBS, centrifuged in 1.5 mL Eppendorf tube at 1000 rpm – 4°C and cell pellet harvested with 30 µL of transmembrane protein lysis buffer (stock: 10 mM Tris-HCl pH 7.5, 0.1 mM EGTA, 0.1 mM EDTA, 0.5% SDS, H_2O; lysis buffer: 1 mL stock lysis buffer, 30 µL Phosphate Inhibitor Cocktail (PIC, Roche), 30 µL Phosphate Inhibitor Buffer (PIB: 25 mM Na_3VO_4, 250 mM Para-NitroPhenyl Phosphate, 250 mM β-glycerophosphate, 125 nM NaF), 2 μL of β-mercaptoethanol 0.2%). After 15 min of incubation on ice, the samples were sonicated for 3 times 10 seconds and stored at -80°C.

Western blotting

Quantification of proteins was carried out using Pierce 660 nm Protein assay (Thermo Fisher Scientific). The protein concentration was determined using the calibration curve (0 to 2 µg/µL bovine serum albumin). Equal protein loading (7 µg) was further confirmed by α-tubulin revelation.

Protein were separated on 10 % homemade polyacrylamide gel composed of 4 % stacking gel (1.25 mL concentration buffer (0.5 M Tris, 0.4 % sodium dodecylsulfate (SDS), pH 6.8), 0.5 mL acrylamide 30 %, 2.25 mL distilled water, 50 μL ammonium persulphate (APS) 10 %, 5 μL of tetramethylethylenediamine (TEMED)) and a 10 % separating gel (1.2 mL staking buffer (1.5 M Tris, 0.4 % SDS, pH 8.8), 1.7 mL acrylamide 30 %, 2.1 mL of distilled water, 25 μL APS 10 %, 5 μL of TEMED).

For each sample, 7 µg of proteins were mixed with 6 μL of loading blue 5X (10 mL concentration buffer, 10 mL SDS 20 %, 5 mL of β-mercaptoethanol, 10 mL of glycerol, 17.5 mg of bromophenol blue, pH 6.8) and bidistilled water up to 30 μL, heated for 5 minutes at 100°C and span briefly. 30 µL of each sample were loaded in gel wells (7 µg protein diluted in bidistilled water) or 2 μL of molecular-weight size marker (New England Biolabs). The migration was performed in a migration tank containing 1 L of running buffer 1X (2.5 mM Tris, 19.2 mM glycine, 5 mL SDS 20%) at 200 V, 400 mA and 15 W per gel, until the migration front reached the bottom of the running buffer gel.

Proteins were transferred from the gel onto a PVDF membrane (Bio-Rad), which was previously hydrated 1 min in methanol 100 % and 3 min in transfer buffer (Bio Rad), using Trans-Blot Turbo transfer cassette (Bio-Rad). The transfer was executed following the manufacturer instruction at 2.5 amperes and 25 volts for 7 minutes.

Blots were incubated with Odyssey blocking buffer (Li-Cor Biosciences) diluted 1/2 in PBS at room temperature for 1 h. The membranes were incubated overnight at 4°C with primary monoclonal antibodies in blocking buffer completed with Tween 20 (Bio-Rad) 0.1 %. After rinsing with PBS – Tween 20 0.1% (3 × 5 minutes), membranes were incubated with secondary antibodies for 1h, rinsed with PBS (3 × 5 minutes), dried and scaned using Odyssey imaging system (Li-Cor Biosciences). Quantification of bands was made using Odyssey software and relative protein quantification was standardized to tubulin abundance.

Immunofluorescence labeling

In 24 well plates (Corning) with uncoated or 1 µg/cm^2 fibronectin (Sigma) coated cover-slips (c.o. - Glaswarenfabrik Karl Hecht KG), 0.025 * 10^6 MDA-MB-231 cells were seeded, in RPMI-1640 medium containing L-glutamate supplemented with 10 % fetal bovine serum, 48h before 10 min paraformaldehyde 4 % fixation (Merck). After PBS washing (3 × 10 minutes), cells were permeabilized 5 min with PBS-Triton 1 % (*Triton X-100* - Carl Roth), washed with PBS-BSA 2 % (Bovine serum albumin – VWR) and incubated with primary antibodies diluted in PBS-BSA 2% overnight at 4°C in dark and humidified chamber. After being washed with PBS-BSA 2 % (3 × 10 min), cells were incubated for 1 hour at room temperature in dark with secondary antibodies, Hoechst (H-21491 -Thermo Fisher Scientific) and probe. Cells were washed in PBS-BSA 2 % and in PBS (2 × 5 minutes) and cover slips were mounted on microscope slides (VWR) with Mowiol mounting solution (Sigma-Aldrich) prewarmed at 56°C. Slides were kept at 4°C protected from light before the observation with the confocal laser scanning fluorescence microscope TCS SP5 (Leica).

Wound healing assay

In 35 mm x 10 mm polystyrene cell culture dish (Corning), 0.8 * 10^6 MDA-MB-231 cells were seeded for 24h at 37°C – 5 % CO_2 to obtain an over confluent cell layer, in RPMI-1640 medium containing L-glutamate supplemented with 10 % fetal bovine serum. The confluent cell layer was scraped to form an ~1 mm width wound. Fresh complete medium supplemented with 10 µg/mL mitomycin C (Sigma-Aldrich) was added to the scraped cells. Live imaging in incubator at 37°C – 10 % CO_2 was monitored using Cytonote holographic system (Iprasense – *Horus* software), taking pictures each 20 minutes during 48h. Relative speed of migration and closing areas were determined using *ImageJ – Phase Wound Macro*.

Preparation of the IGDQ-exposing surface gradients

Gold surfaces (2 nm Ti, 10 nm Au on glass coverslips), produced by physical vapor deposition at the LARN (UNamur) using plasma deposition chamber (*ATC-Orion 5 UHV with Load-Lock* – AJA International Inc.) and were then cleaned with UV – Ozone (2h - organic compounds removing). The IGDQ-exposing surface gradients on gold were prepared following our previously reported protocol [27] using a tetraethylenglycol-based terminal thiol (PS – Figure 1B–1C) as the filler. After EtOH cleaning, the surfaces were placed into 24 well plates and a 0.6 µL drop containing cells at 1 * 10^6 cells/mL was deposited to seed the cells at the lower concentration of IGDQ. 4 min later, wells were filled with RPMI-1640 medium containing L-glutamate supplemented with 10% fetal bovine serum. Cell migration was monitored using Ovizio v1.0 holographic microscopy (*Ovizio Imaging System* – OsOne v5.1) once a day for 5 days (Figure 1C).

Mass spectrometry protein analysis

MDA-MB-231 cells grown in T75 flask (1 * 10^6 cells for 48h) were washed with PBS on ice, scraped off the plastic surface in PBS, centrifuged in 1.5 mL Eppendorf tube at 1000 rpm – 4°C and cell pellet harvested with 60 µL of DLA lysis buffer (in 25mL bidistilled water – pH 7.5: 7 M urea,

2 M thiolurea, 30 mg tris-EDTA, 1 % CHAPS) and kept at -80°C. Protein quantification was determined using Pierce 660 nm Protein assay as described for western blotting. For all conditions, four biological independent replicates were generated.

Protein lysates were processed based on the multienzyme digestion-filter aided sample preparation (MED-FASP) using Microcon 30k centrifugal ultrafiltration units (Millipore). At 24°C, 50 µg of proteins were reduced with 1 M DTT (dithiothreitol) and alkylated with 550 mM iodoacetamide [50]. Subsequently, samples were digested overnight with 1 µg of a mix LysC (Wako) / Trypsin (Trypsin Gold Promega) in 1 M urea. Samples were subjected to centrifugation and dried using speed-vacuum (Heto). Peptides were resuspended in 300 μl of trifluoroacetic acid 0.1 % (TFA - Biosolve). Subsequently, peptides were subjected to *Pierce High pH Reversed-Phase Peptide Fractionation* Kit (# 84868 -Thermo Scientific) following supplier's instructions. In short, columns were rinsed and equilibrated, samples were loaded and peptides were eluted in 8 fractions with acetonitrile gradient (ACN – 5, 7.5, 10, 12.5, 15, 17.5, 20 and 50 %) in TFA 0.1 %. Fractions were then dried and resuspended in formic acid 1 % (Biosolve).

Each of the 8 fractions was separately analyzed using an ESI-MS/MS maXis Impact UHR-TOF (Bruker) coupled with an UltiMate 3000 nanoUPLC system (Thermo Scientific). The digests were separated by reverse-phase liquid chromatography using a 75 μm × 250 mm reverse phase column (Ac- claim PepMap 100 C18, Thermo Scientific). Mobile phase A was 9 5% water −5 % acetonitrile, 0.1 % formic acid. Mobile phase B was 20% water−80 % acetonitrile, 0.1 % formic acid . The samples were injected and the organic content of the mobile phase was increased from 4 % B to 25 % B in 60 min, from 25 % B to 40 % B in 25min, from 40 % to 90 % in 5 min and then washed with 90 % B for 10 min, for a total of 120 min. The column effluent was connected to a Captive Spray (Bruker). In survey scan, MS spectra were acquired for 0.5 second in the mass to charge (m/z) range between 50 and 2200. The most intense peptide ions 2+ to 4+ were sequenced during a cycle time of 3 seconds. The collision-induced dissociation energy was automatically set according to m/z ratio and charge state of the precursor ion. The maXis and the Ultimate were controlled by Compass Hystar 3.2 (Bruker). Three independent biological replicates for each condition were analyzed.

Tandem mass spectra were extracted and charge state deconvoluted by Data Analysis v.4.2 (Bruker). MGF peak lists obtained from MS/MS spectra for all fractions from a sample were loaded In Scaffold v.4.8 (Proteome Software Inc.) as MUDPIT experiments in which case, the analysis combines peptides from all fractions into one MS sample for protein identification [51]. MGF peak lists were identified using Mascot v.2.5.1 (Matrix Science) and X! Tandem v.CYCLONE 2010.12.01.1 (The GPM, thegpm.org). Mascot was set up to search the Uniprot-Homo Sapiens and isoform_190904 database (195195 entries) assuming the digestion enzyme trypsin. X! Tandem was set up to search a reverse concatenated subset of the Uniprot-HomoIsoform_190904 database. Mascot and X!Tandem were searched with a fragment ion mass tolerance of 0.050 Da and a parent ion tolerance of 10.0 ppm. Carbamidomethyl of cysteine was specified in Mascot and X! Tandem as fixed modifications. Gln->pyro-Glu of the N-terminus and oxidation of methionine were specified in Mascot and X! Tandem as variable modifications.

Scaffold v.4.8 (Proteome Software Inc.) was used to validate MS/MS based peptide and protein identifications [53]. Peptide identifications were accepted if they could be established at greater than 80 % probability to achieve an FDR less than 1 % by the Scaffold Local FDR algorithm. Protein identifications were accepted if they could be established at greater than 5 % probability (p-value < 0.05) to achieve an FDR less than 1 % and contained at least 3 identified peptides. Protein probabilities were assigned by the Protein Prophet algorithm [52]. Proteins that contained similar peptides and could not be differentiated based on MS/MS analysis alone were grouped into clusters.

Relative protein abundance was determined using the total spectral counts obtained in the sample for each protein cluster, containing same protein variants. The differential expression was determined after a t-test (p-value < 0.05, no correction – Scaffold software) comparing control condition (shCTL) to shA5-126 or shB3-237. Protein links and gene ontology (GO) enrichment were performed using STRING (*Expasy* tool, consulted on 2020-01).

Statistics

Each experiment was performed in at least three independent replicates. Data from mRNA, protein and cell migration are presented as mean ± SD. Two-way ANOVA was performed followed by the post-hoc Bonferroni test. Data from relative migration speed were analyzed using an unpaired t-test with Welch's correction. Significant p-value are presented as follow: $p < 0.05$, $^{**}p < 0.01$ and $^{***}p < 0.001$ (*GraphPad Prism 5* v.5.01).

Differential expression from mass spectrometry analysis was obtained from total spectral counts and t-test with p-value < 0.05 (no correction) was performed to compare knock-down cells to control cells (shCTL vs shA5-126 or shCTL vs shB3-237) using the *Scaffold* software.

Author contributions

S.A.C. designed, conducted, and analyzed the experiments, interpreted the experimental data, created the figures and wrote the manuscript with the assistance from C.M., D.B., R.T., L.P. and M.D.. R.T. designed the experiments and produced peptides. L.P. designed and analyzed the experiments and interpreted the experimental data. C.D. prepared samples for mass spectrometry analysis. M.D. performed mass spectrometry sample analysis and bioinformatics analysis. A.F. performed real-time qPCR experiments. S.L. and T.T. supervised and conducted gold surface production. C.M and D.B. developed the concept, led and supervised the studies.

Acknowledgments

This work was supported by the Fonds National pour la Recherche Scientifique (FNRS - Belgium) [T.1112.14; 2014]; the School of Chemistry at Cardiff University (UK), the University of Namur (BE) and NARILIS research institute (BE). The authors are thankful to UNamur technological platforms: MaSUN, SIAM and Morph-Im.

Supplementary materials

Supplementary material associated with this article can be found, in the online version, at doi:10.1016/j.neo.2022.100816.

References

[1] Siegel RL, Miller KD, Fuchs HE, Jeam A. Cancer Statistics, 2021. *Cancer Statistics* 2021;**71**:7–33.

[2] Aman A, Piotrowski T. Cell migration during morphogenesis. *Developmental Biology* 2010;**341**:20–33.

[3] Friedl P, Hegerfeldt Y, Tusch M. Collective cell migration in morphogenesis and cancer. *Int. J. Dev. Biol.* 2004;**48**:441–9.

[4] Vaezi A, Bauer C, Vasioukhin V, Fuchs E. Actin cable dynamics and Rho/Rock orchestrate a polarized cytoskeletal architercture in the early steps of assembling a stratified epithelium. *Dev. Cell* 2002;**3**:367–81.

[5] Werner S, Krieg T, Smola H. Keratinocyte-fibroblast interactions in wound healing. *J. Invest. Dermatol.* 2007;**127**:998–1008.

[6] Szurmant H, Ordal GW. Diversity in Chemotaxis Mechanisms among the Bacteria and Archaea. *Microbiol. Mol. Biol. Rev.* 2004;**68**:301–19.

[7] Trepat X, Chen Z, Jacobson K. Cell Migration. *Comprehensive Physiology* 2012;**2**:2369.

[8] Frantz C, Stewart KM, Weaver VM. The extracellular matrix at a glance. *Journal of Cell Science* 2010;**123**:4195–200.

[9] Doyle AD, Carvajal N, Jin A, Matsumoto K, Yamada KM. Local 3D matrix microenvironment regulates cell migration through spatiotemporal dynamics of contractility-dependent adhesions. *Nat. Commun.* 2015;**6**.

[10] Ma X, et al. Fibers in the extracellular matrix enable long-range stress transmission between cells. *Biophys. J.* 2013;**104**:1410–18.

[11] Wang H, Abhilash AS, Chen CS, Wells RG, Shenoy VB. Long-range force transmission in fibrous matrices enabled by tension-driven alignment of fibers. *Biophys. J.* 2015;**107**:2592–603.

[12] Varennes J, Moon Hran, Saha S, Mugler A, Han B. Physical constraints on accuracy and persistence during breast cancer cell chemotaxis. *PLoS Comput. Biol.* 2019;**15**:e1006961.

[13] Franca-Koh J, Devreotes PN. Moving Forward: Mechanisms of Chemoattractant Gradient Sensing. *Physiology* 2004;**19**:300–8.

[14] Brenner MP, Levitov LS, Budrene EO. Physical mechanisms for chemotactic pattern formation by bacteria. *Biophys. J.* 1998;**74**:1677–93.

[15] Wang SJ, Saadi W, Lin F, Minh-Canh Nguyen C, Li Jeon N. Differential effects of EGF gradient profiles on MDA-MB-231 breast cancer cell chemotaxis. *Exp. Cell Res.* 2004;**300**:180–9.

[16] Hartman CD, Isenberg BC, Chua SG, Wong JY. Vascular smooth muscle cell durotaxis depends on extracellular matrix composition. *Proc. Natl. Acad. Sci. U. S. A.* 2016;**113**:11190–5.

[17] Pankov R, Yamada KM. Fibronectin at a glance. *J. Cell Sci.* 2002;**115**:3861–3.

[18] Ffrench-Constant C. Alternative splicing of fibronectin - Many different proteins but few different functions. *Experimental Cell Research* 1995;**221**:261–71.

[19] Schor S, Ellis I, Banyard J, Schor A. Motogenic activity of IGD-containing synthetic peptides. *J. Cell Sci.* 1999;**112**:3879–88.

[20] Pereira AM, et al. Silk-based biomaterials functionalized with fibronectin type II promotes cell adhesion. *Acta Biomater* 2017;**47**:50–9.

[21] Forastieri H, Ingham KC. Interaction of gelatin with a fluorescein-labeled 42-kDa chymotryptic fragment of fibronectin. *J. Biol. Chem.* 1985;**260**:10546–10550.

[22] Mao Y, Schwarzbauer JE. Fibronectin fibrillogenesis, a cell-mediated matrix assembly process. *Matrix Biology* 2005;**24**:389–99.

[23] Ruoslahti E, Pierschbacher MD. New Perspectives in Cell Adhesion: RGD and Integrins. *Science* 1987;**238**(80-):491–7.

[24] Takada Y, Ye X, Simon S. The integrins. *Genome Biol* 2007;**8**:215.

[25] Mrksich M. Tailored substrates for studies of attached cell culture. *Cellular and Molecular Life Sciences* 1998;**54**:653–62.

[26] Smith JT, et al. Measurement of cell migration on surface-bound fibronectin gradients. *Langmuir* 2004;**20**:8279–86.

[27] Bhat RR, Chaney BN, Rowley J, Liebmann-Vinson A, Genzer J. Tailoring cell adhesion using surface-grafted polymer gradient assemblies. *Adv. Mater.* 2005;**17**:2802–7.

[28] Schor SL, et al. Substratum-dependent stimulation of fibroblast migration by the gelatin-binding domain of fibronectin. *J. Cell Sci.* 1996;**109**(Pt 1):2581–90.

[29] Millard CJ, et al. The role of the fibronectin IGD motif in stimulating fibroblast migration. *J. Biol. Chem.* 2007;**282**:35530–5.

[30] Damsky WE, Theodosakis N, Bosenberg M. Melanoma metastasis: new concepts and evolving paradigms. *Oncogene* 2014;**33**:2413–22.

[31] Corvaglia V, Marega R, De Leo F, Michiels C, Bonifazi D. Unleashing Cancer Cells on Surfaces Exposing Motogenic IGDQ Peptides. *Small* 2016;**12**:321–9.

[32] Barreiro O, Martín P, González-Amaro R, Sánchez-Madrid F. Molecular cues guiding inflammatory responses. *Cardiovasc. Res.* 2010;**86**:174–82.

[33] Kiosses WB, Shattil SJ, Pampori N, Schwartz MA. Rac recuits high-affinity integrin αvβ3 to lamellipodia in endothelial cell migration. *Nat. Cell Biol.* 2001;**3**:316–20.

[34] De Franceschi N, Hamidi H, Alanko J, Sahgal P, Ivaska J. Integrin traffic - the update. *J. Cell Sci.* 2015;**128**:839–52.

[35] Maurer LM, Annis DS, Mosher DF. IGD motifs, which are required for migration stimulatory activity of fibronectin type I modules, do not mediate binding in matrix assembly. *PLoS One* 2012;**7**.

[36] Ciarrocchi A, Rieber MS, Rieber M. Extracellular RGD-binding proteins modulate cell adhesion. *Biochem. Biophys. Res. Commun.* 1992;**183**:544–52.

[37] Chicurel ME, Singer RH, Meyer CJ, Ingber DE. Integrin binding and mechanical tension induce movement of mRNA and ribosomes to focal adhesions. *Nature* 1998;**392**:730–3.

[38] Willett M, Flint SA, Morley SJ, Pain VM. Compartmentalisation and localisation of the translation initiation factor (eIF) 4F complex in normally growing fibroblasts. *Exp. Cell Res.* 2006;**312**:2942–53.

[39] Willett M, Pollard HJ, Vlasak M, Morley SJ. Localization of ribosomes and translation initiation factors to talin/β3-integrin-enriched adhesion complexes in spreading and migrating mammalian cells. *Biol. Cell* 2010;**102**:265–76.

[40] Missirlis D, et al. Substrate engagement of integrins α5 β1 and αv β3 is necessary, but not sufficient, for high directional persistence in migration on fibronectin. *Sci. Rep.* 2016;**6**:1–18.

[41] Caswell PT, et al. Rab-coupling protein coordinates recycling of α5β1 integrin and EGFR1 to promote cell migration in 3D microenvironments. *J. Cell Biol.* 2008;**183**:143–55.

[42] Roberts M, Barry S, Woods A, Van der Sluijs P, Norman J. PDGF-regulated rab4-dependent recycling of αvβ3 integrin from early endosomes is necessary for cell adhesion and spreading. *Curr. Biol.* 2001;**11**:1392–402.

[43] Reynolds AR, et al. Stimulation of tumor growth and angiogenesis by low concentrations of RGD-mimetic integrin inhibitors. *Nat. Med.* 2009;**15**:392–400.

[44] Steinberg F, Heesom KJ, Bass MD, Cullen PJ. SNX17 protects integrins from degradation by sorting between lysosomal and recycling pathways. *J. Cell Biol.* 2012;**197**:219–30.

[45] Margadant C, Kreft M, De Groot DJ, Norman JC, Sonnenberg A. Distinct roles of talin and kindlin in regulating integrin α5β1 function and trafficking. *Curr. Biol.* 2012;**22**:1554–63.

[46] Morgan MR, et al. Syndecan-4 Phosphorylation Is a Control Point for Integrin Recycling. *Dev. Cell* 2013;**24**:472–85.

[47] Caswell P, Norman J. Endocytic transport of integrins during cell migration and invasion. *Trends in Cell Biology* 2008;**18**:257–63.

[48] Weidle UH, Birzele F, Kollmorgen G, Rüger R. The multiple roles of exosomes in metastasis. *Cancer Genomics and Proteomics* 2017;**14**:1–16.

[49] Paul NR, Jacquemet G, Caswell PT. Endocytic Trafficking of Integrins in Cell Migration. *Current Biology* 2015;**25**:R1092–105.

[50] Wiśniewski JR, Mann M. Consecutive proteolytic digestion in an enzyme reactor increases depth of proteomic and phosphoproteomic analysis. *Anal. Chem.* 2012;**84**:2631–7.

[51] Schirmer EC, Yates-Iii JR, Gerace L. MudPIT: A Powerful Proteomics Tool for Discovery. *Discov. Med.* 2009;**2**:38–9.

[52] Nesvizhskii AI, Keller A, Kolker E, Aebersold R. A statistical model for identifying proteins by tandem mass spectrometry. *Anal. Chem.* 2003;**75**:4646–58.

[53] Searle BC. Scaffold: A bioinformatic tool for validating MS/MS-based proteomic studies. *Proteomics* 2010;**6**:1265–9.